Supporting information

for

Modulating Local Electronic Structure Enhances Superior Electrochemical Activity in Li-Rich Oxide Cathodes

Xin-Yu Li[a], Fu-Da Yu[b,*], Wang Ke[a], Yun-Shan Jiang[a], Lan-Fang Que[b], Lei Zhao[a,*], Su-E Hao[a,*], Zhen-Bo Wang[a,c,*]

[a] MIIT Key Laboratory of Critical Materials Technology for New Energy Conversion and Storage, State Key Lab of Urban Water Resource and Environment, School of Chemistry and Chemical Engineering, Harbin Institute of Technology, Harbin 150001, China

[b] Engineering Research Center of Environment-Friendly Functional Materials, Ministry of Education, Institute of Materials Physical Chemistry, Huaqiao University, Xiamen 361021, China

[c] College of Materials Science and Engineering, Shenzhen University, Shenzhen 518071, China

* Corresponding authors

E-mail addresses: yufuda@hqu.edu.cn (Fu-Da Yu), leizhao@hit.edu.cn (Lei Zhao), haosue@hit.edu.cn (Su-E Hao), wangzhb@hit.edu.cn (Zhen-Bo Wang)

Contents:

is not in contact with the electrolyte, Pristine represents that the electrode is in contact with the electrolyte.

Fig. S13 XRD patterns of B-LMO-400, B-LMO-500, B-LMO-600, B-LMO-700 and B-LMO-800 after 300 cycles at 1 C.

Fig. S14 TEM images of (a,d,g) B-LMO-600, (b,e,h) B-LMO-700 and (c,f,i) B-LMO-800 after 300 cycles at 1 C.

Fig. S15 EPR spectra for B-LMO-600 of Pristine and PVDF with Super-P electrodes. PVDF with Super-P represents that the electrode without active materials.

Table S1 Rietveld refinements results of XRD patterns for LMOs using a monoclinic *C2/m* space group.

Table S2 Cycling performances of B-LMO-400, B-LMO-500, B-LMO-600, B-LMO-700 and B-LMO-800 at 1 C, all cells were activated in three cycles at 0.1 C.

Experimental sections

Materials preparation: Li_2MnO_3 was prepared by the mechanical thermal activation engineering strategy. Frist, Li_2CO_3 and Mn_2O_3 were mixed in the air at the molar ratio of 2:1 for the target composition of Li: Mn = 2:1. Then, the mixture was calcined in an alumina crucible in the air for 10 h at 800℃ (LMO). Next, LMO was subsequently milled using a ball mill in a zirconia pot with zirconia balls with the weight ratio of 1:20 at 500 rpm for 10 h in the air (B-LMO). Finally, B-LMO was further calcined at 400℃, 500℃, 600℃, 700℃, 800℃ for 10 h in the air, respectively (B-LMO-400, B-LMO-500, B-LMO-600, B-LMO-700, B-LMO-800). LMOs represent samples with different contents of oxygen vacancies, including LMO, B-LMO, B-LMO-400, B-LMO-500, B-LMO-600, B-LMO-700 and B-LMO-800.

Materials characterization: Scanning electron microscope (SEM) images were obtained from the field emission scanning electron microscope (SU-70, Hitachi). X-ray photoelectron spectroscopy (XPS) measurements were conducted on the X-ray photoelectron spectrometer (Kratos Axis Ultra) with Al Kα radiation (1486.6 eV). The binding energy values were calibrated by referencing the C 1s peak at 284.8 eV. Electron paramagnetic resonance (EPR) tests were used to characterize the oxygen vacancies at room temperature and carried out on the EPR spectrometer (EMX plus, Bruker) using ~9.8 GHz resonance frequency with 3.0 G modulation amplitude and a 100.0 kHz modulation frequency. X-ray powder diffraction (XRD) spectra were collected using the X-ray diffractometer (D2 Advance, Bruker) with Cu Kα radiation (λ = 1.54184 Å) at room temperature. The corresponding Rietveld refinements were performed by the TOPAS program. *In-situ* XRD tests were operated with the range of 2θ = 17°~70° with a voltage range of 2.0~4.8 V at 0.5 C. For Li_2MnO_3, 1 C = 230 $mA \cdot g^{-1}$ is assumed [1]. Transmission electron microscope (TEM) images were collected from the field emission transmission electron microscope (JEM-2100). Raman measurements were performed using a 532 nm laser (LabRAM HR Evolution, HORIBA Scientific). UV-vis diffuse

reflectance spectra (UV-vis DRS) tests were performed on the UV-vis absorption spectrophotometer (Lambda750, Perkin Elmer). The reflectance was converted to absorbance via the standard Kubelka-Munk theory. XPS valence band spectra tests were conducted on the X-ray photoelectron spectrometer (Kratos Axis Ultra) with Al Kα radiation (1486.6 eV).

Electrochemical measurement: First, the cathode slurry was prepared by mixing the active materials, Super-P and polyvinylidene fluoride (PVDF) with a mass ratio of 8:1:1 in the 1-methyl-2-pyrrolidone (NMP) solvent. Next, the cathode slurry was uniformly coated on aluminum foil and dried in vacuum at 120 °C. Then punch it into a 14-mm diameter disk. The electrolyte was 1 $mol \cdot L^{-1}$ $LiPF_6$ dissolved in ethylene carbonate (EC) and dimethyl carbonate (DMC) with a volume ratio of 1:1. Lithium metal was used as the anode. The assembly work was conducted in an argon-filled glovebox, and all prepared electrodes and lithium electrodes were installed into CR2025 button cells. Galvanostatic charge/discharge tests were performed on the Neware battery test system with a voltage range of 2.0~4.8 V at room temperature. Electrodes for characterization were prepared by cycling to the desired conditions, then immediately disassembling the cells carefully and washing off the electrolyte residual with DMC [2]. And this is not required for fresh electrodes.

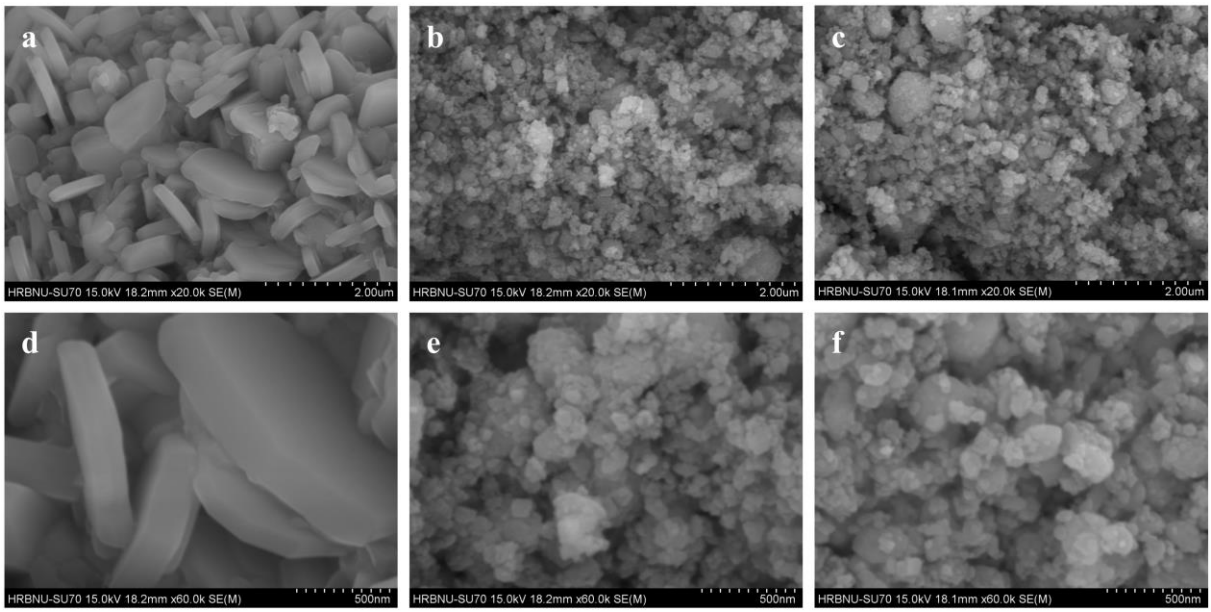

Fig. S1 SEM images of (a,d) LMO, (b,e) B-LMO and (c,f) B-LMO-600.

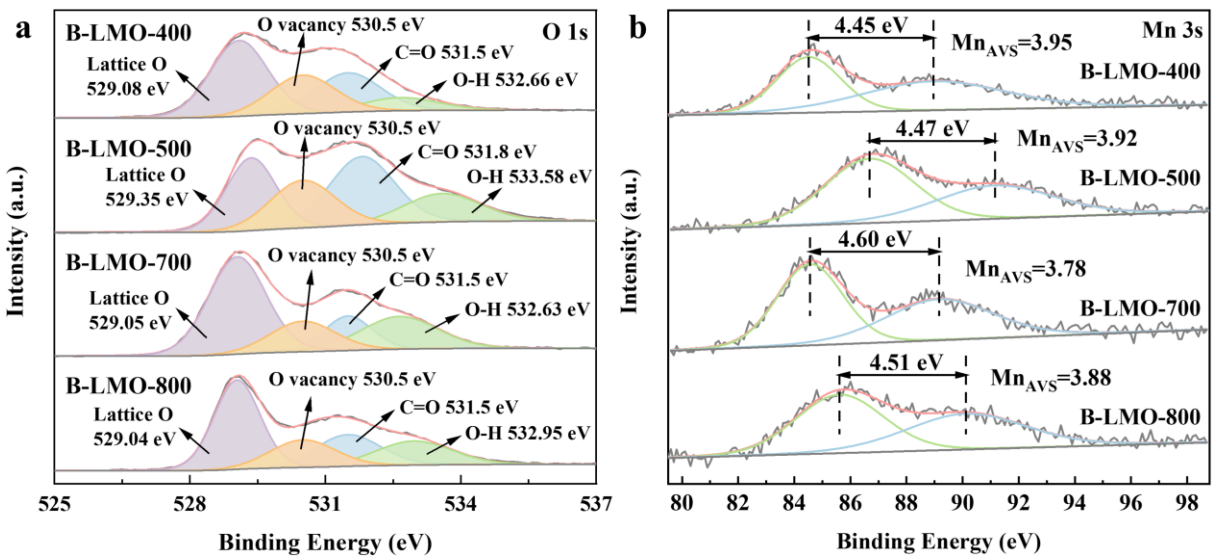

Fig. S2 High-resolution XPS results of (a) O 1s and (b) Mn 3s for B-LMO-400, B-LMO-500, B-LMO-700 and B-LMO-800.

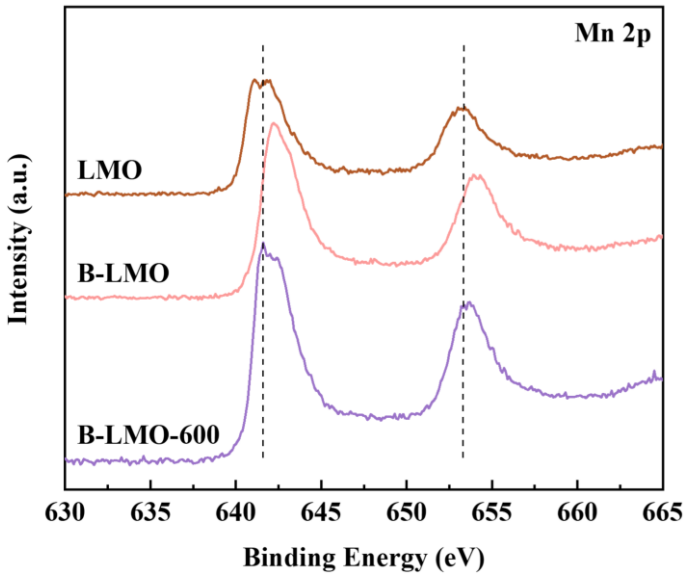

Fig. S3 High-resolution XPS results of Mn 2p for LMO, B-LMO and B-LMO-600.

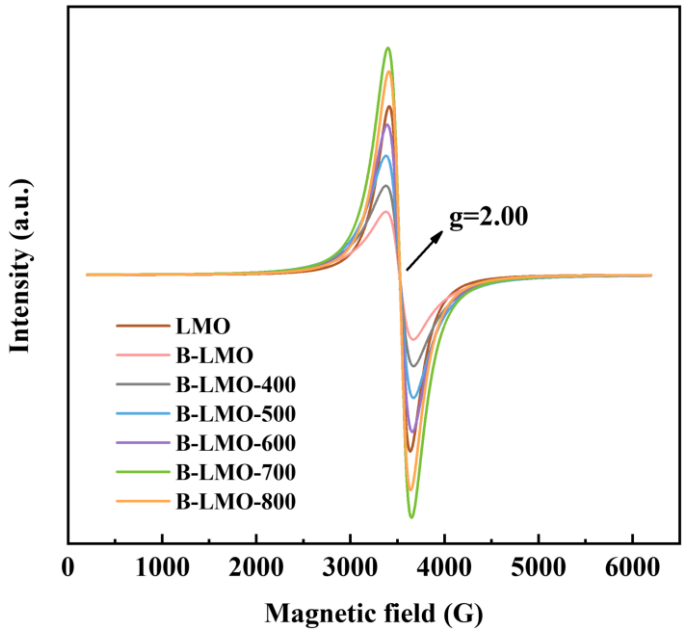

Fig. S4 EPR spectra of LMOs.

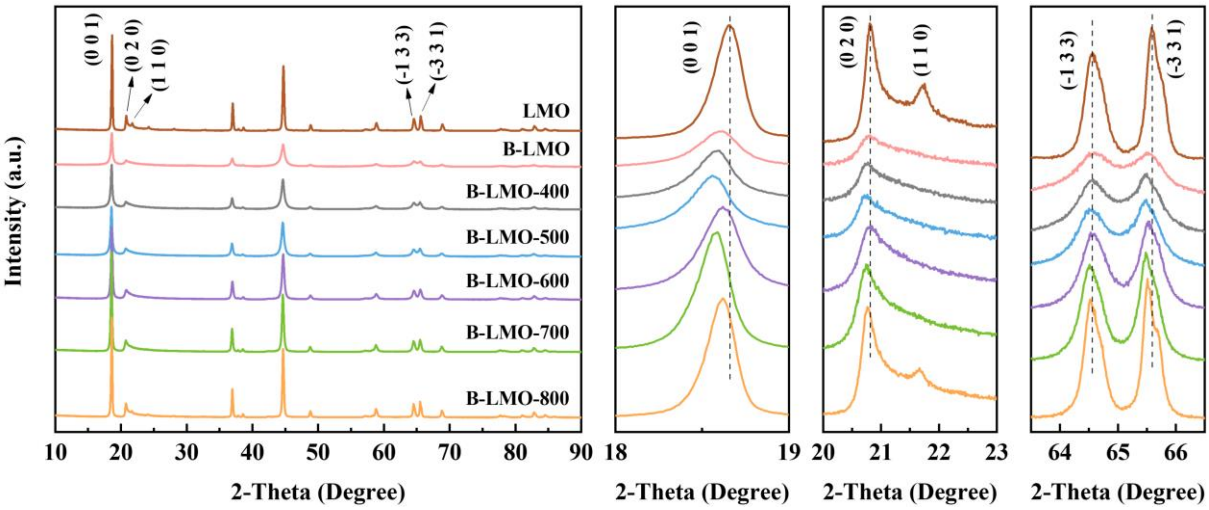

Fig. S5 XRD patterns of LMOs.

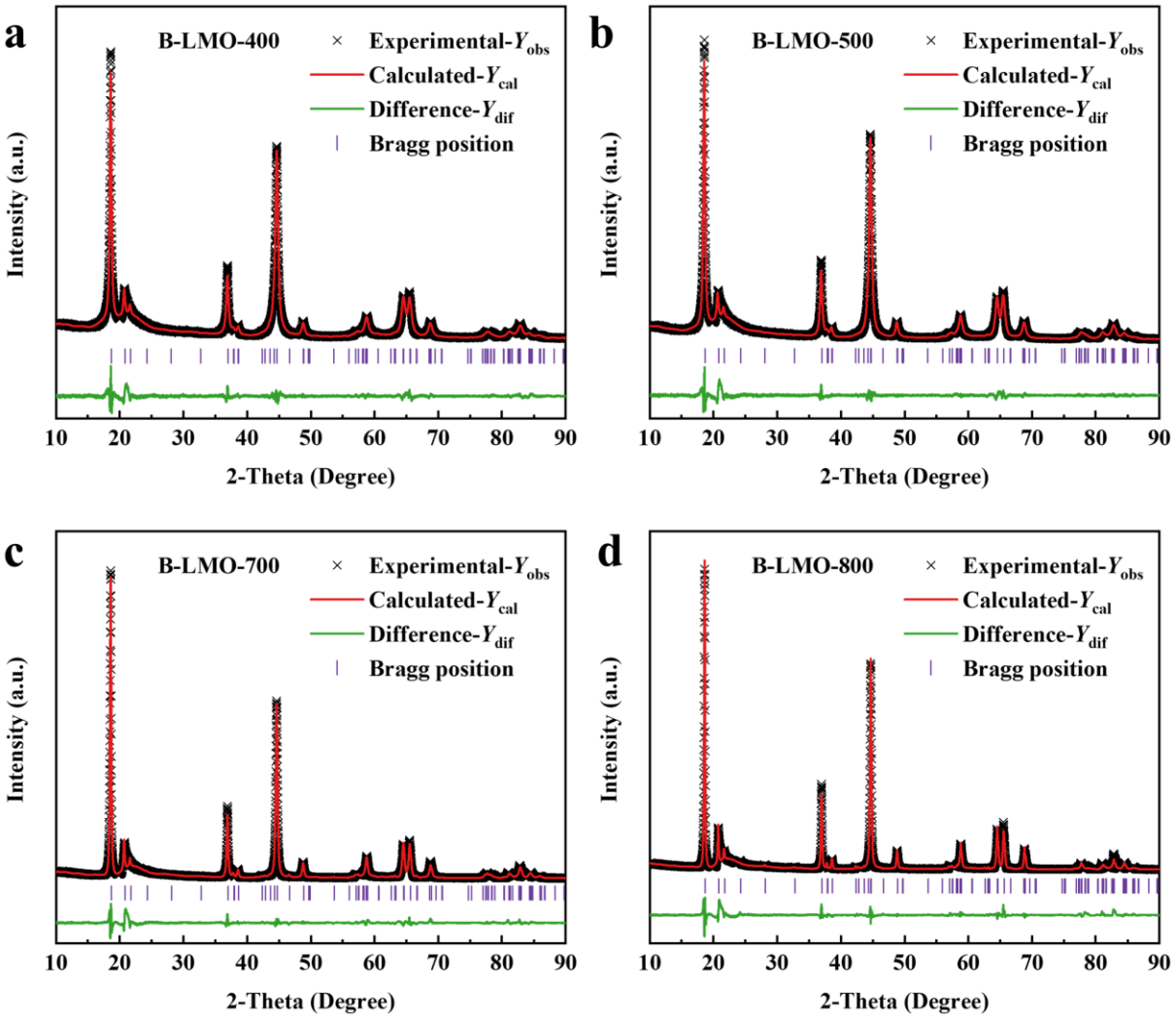

Fig. S6 Rietveld refinement based on the XRD patterns of (a) B-LMO-400, (b) B-LMO-500, (c) B-LMO-700 and (d) B-LMO-800.

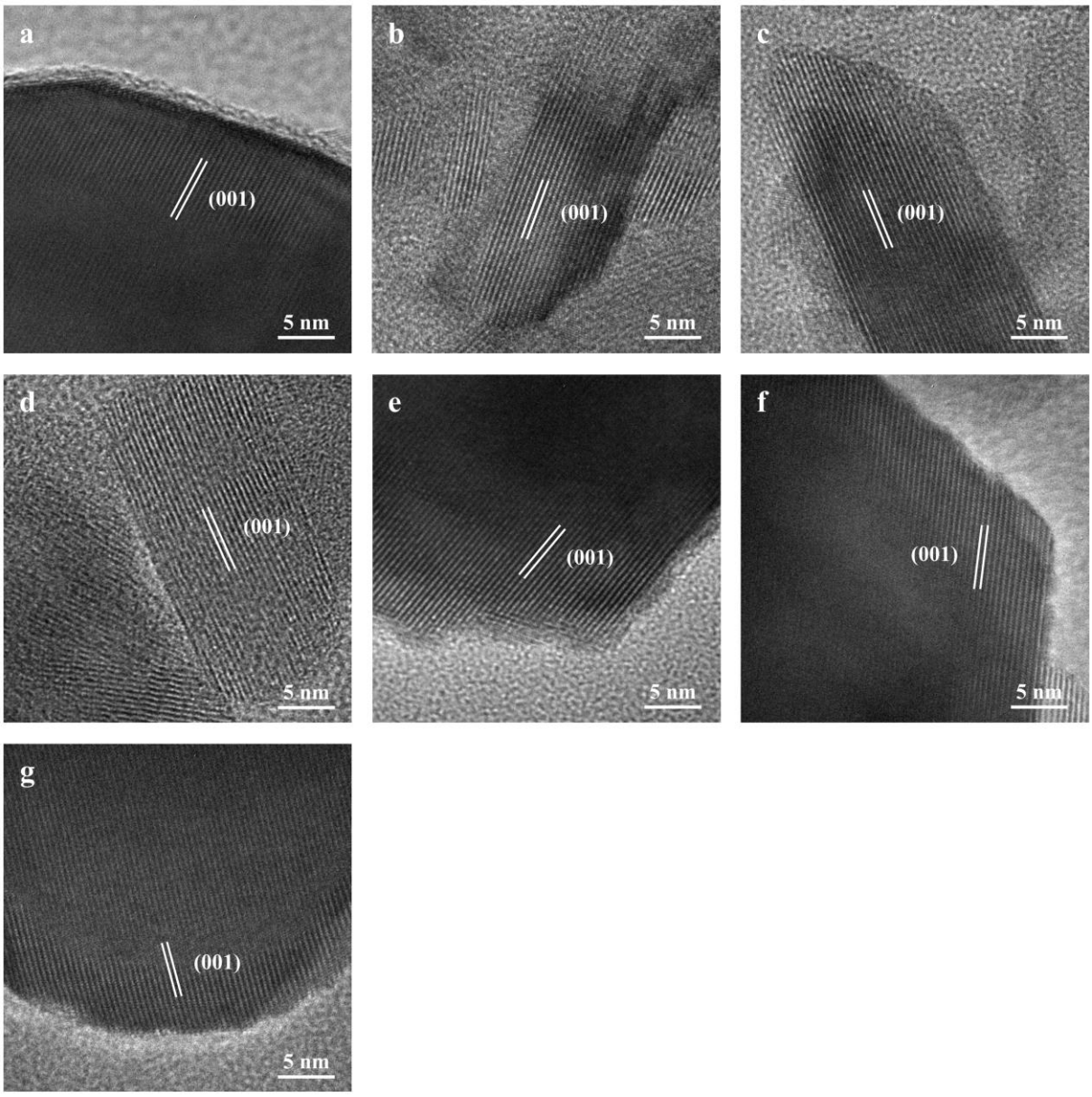

Fig. S7 High-resolution TEM images of (a) LMO, (b) B-LMO, (c) B-LMO-400, (d) B-LMO-500, (e) B-LMO-600, (f) B-LMO-700 and (g) B-LMO-800.

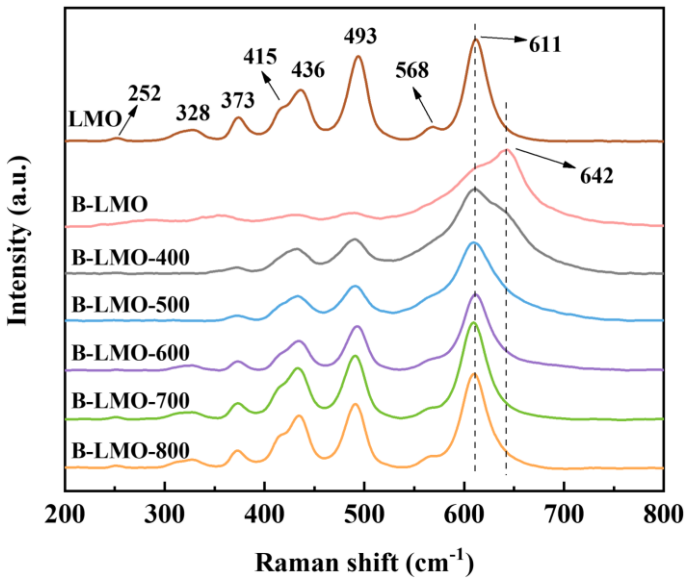

Fig. S8 Raman spectra of LMOs.

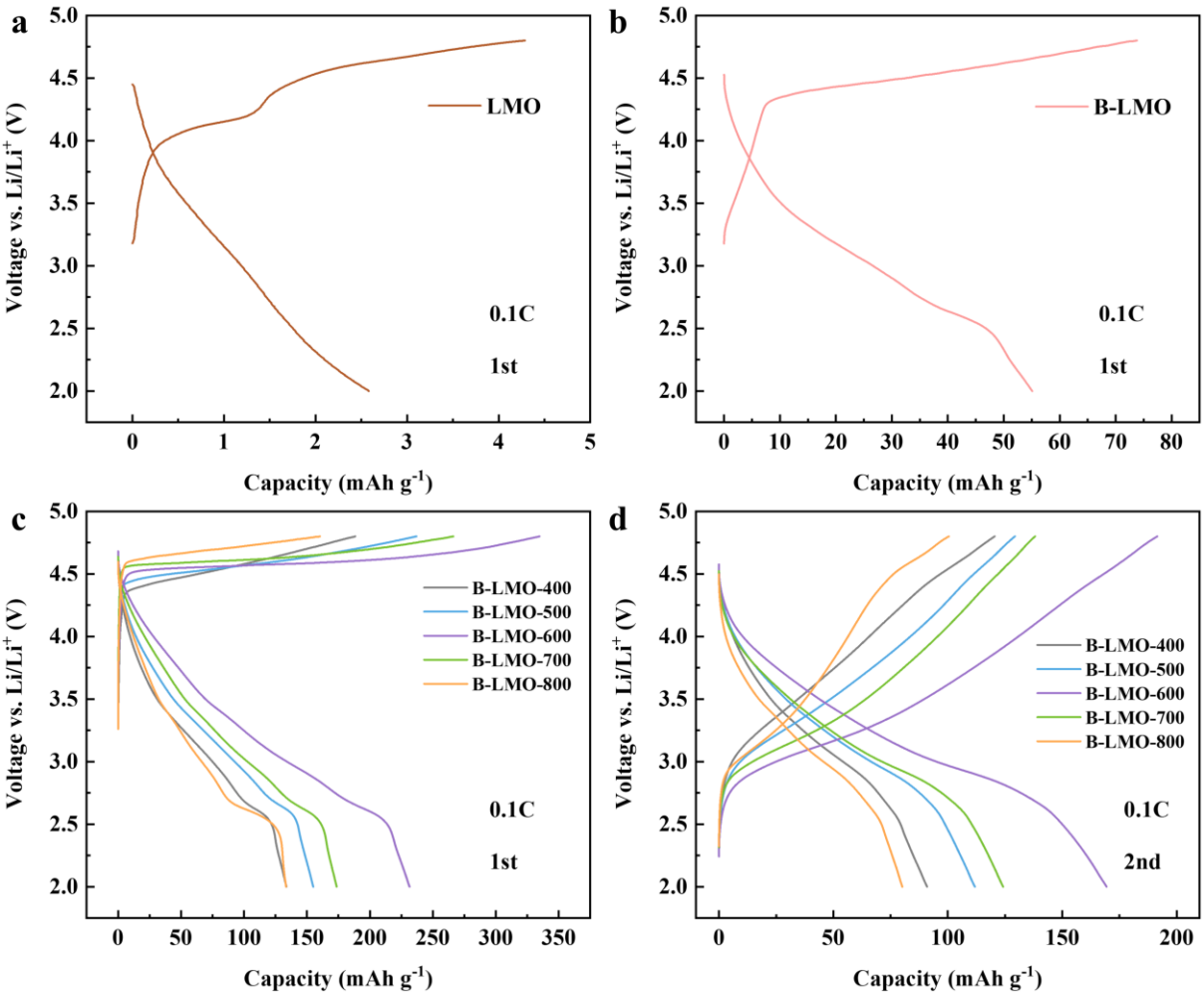

Fig. S9 The first cycle galvanostatic charge/discharge profiles at 0.1 C for (a) LMO, (b) B-LMO, (c) B-LMO-400, B-LMO-500, B-LMO-600, B-LMO-700 and B-LMO-800. (d) The second cycle galvanostatic charge/discharge profiles at 0.1 C for B-LMO-400, B-LMO-500, B-LMO-600, B-LMO-700 and B-LMO-800.

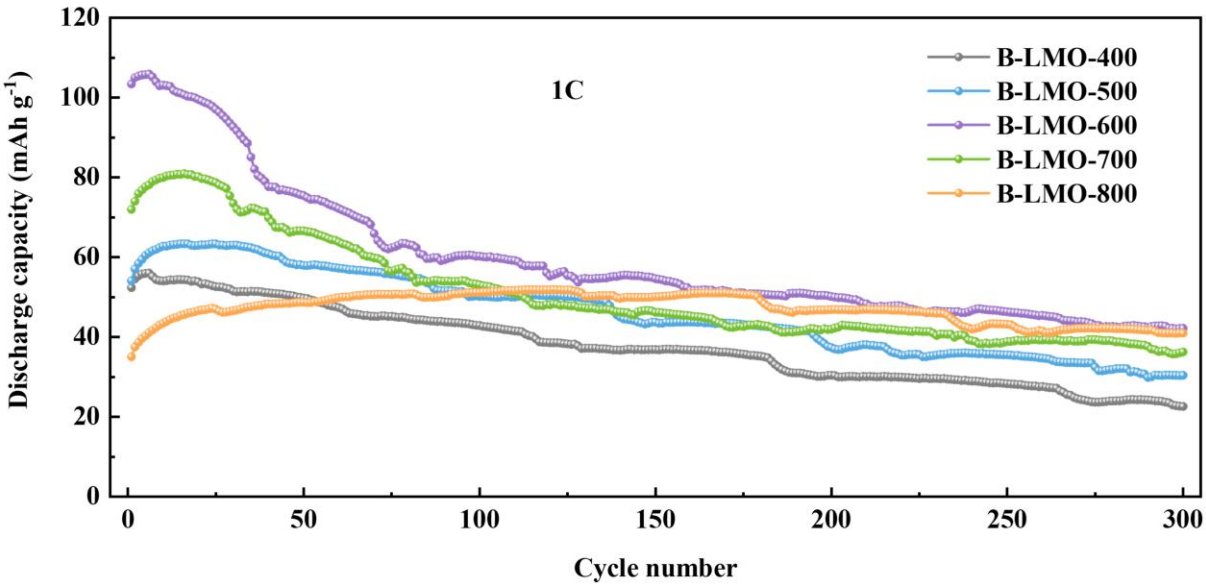

Fig. S10 Cycling performance curves of B-LMO-400, B-LMO-500, B-LMO-600, B-LMO-700 and B-LMO-800 at 1 C, all cells were activated in three cycles at 0.1 C.

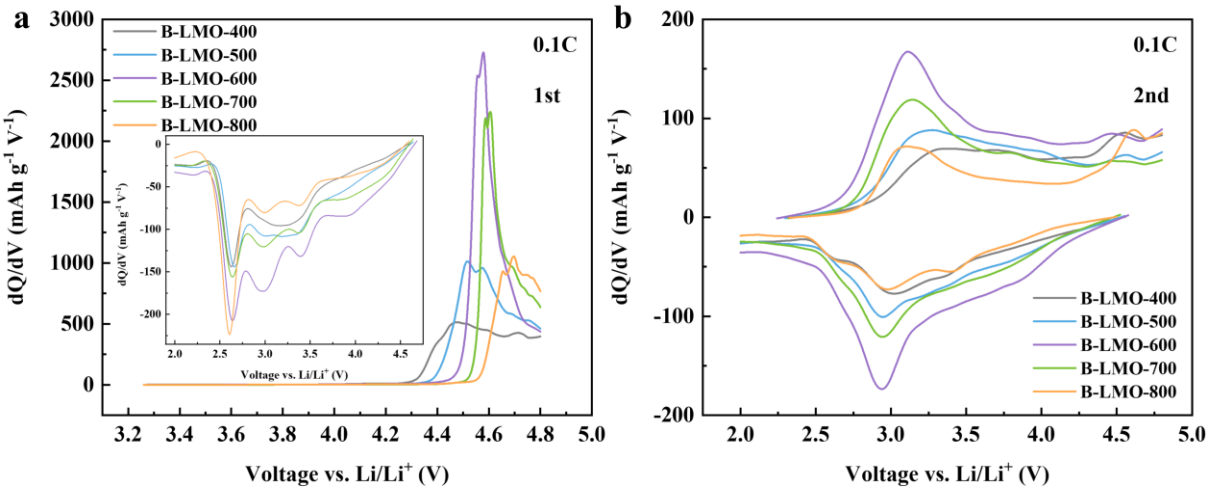

Fig. S11 The dQ/dV curves for B-LMO-400, B-LMO-500, B-LMO-600, B-LMO-700 and B-LMO-800 during (a) the first and (b) the second cycle at 0.1 C.

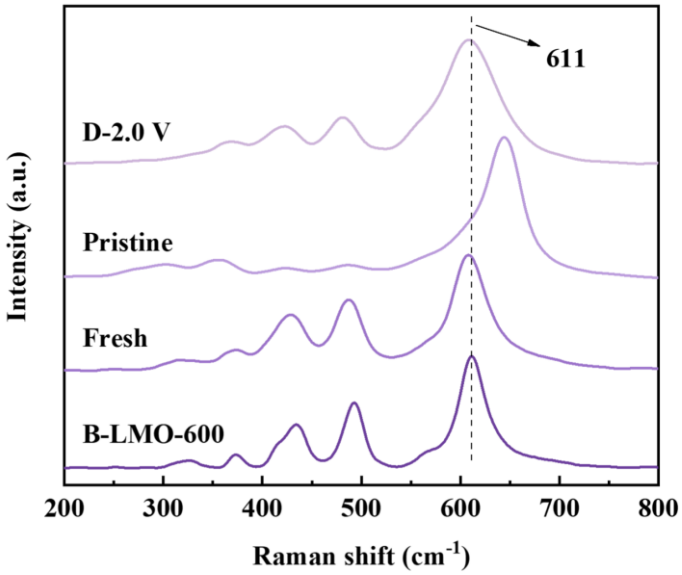

Fig. S12 Raman spectra of Fresh and Pristine electrodes for B-LMO-600. Fresh represents that the electrode is not in contact with the electrolyte, Pristine represents that the electrode is in contact with the electrolyte.

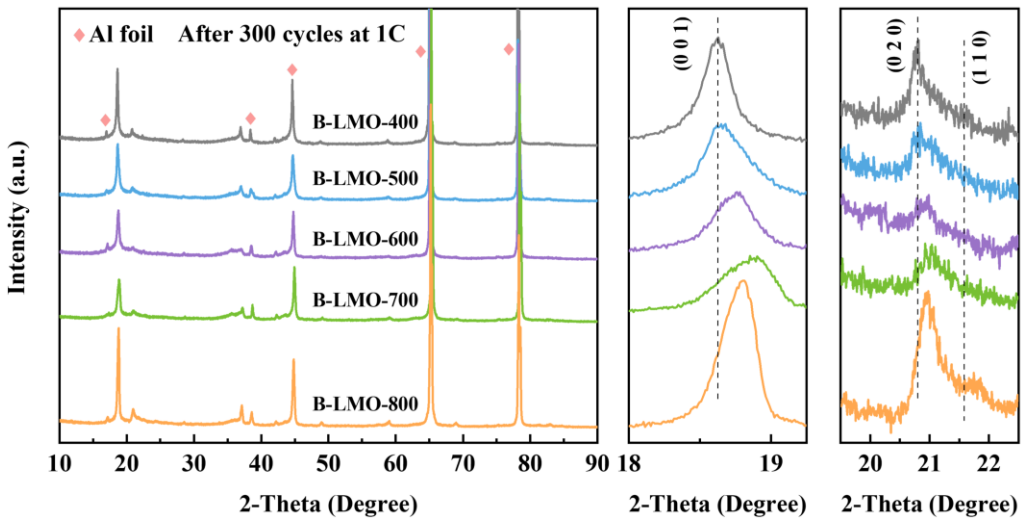

Fig. S13 XRD patterns of B-LMO-400, B-LMO-500, B-LMO-600, B-LMO-700 and B-LMO-800 after 300 cycles at 1 C.

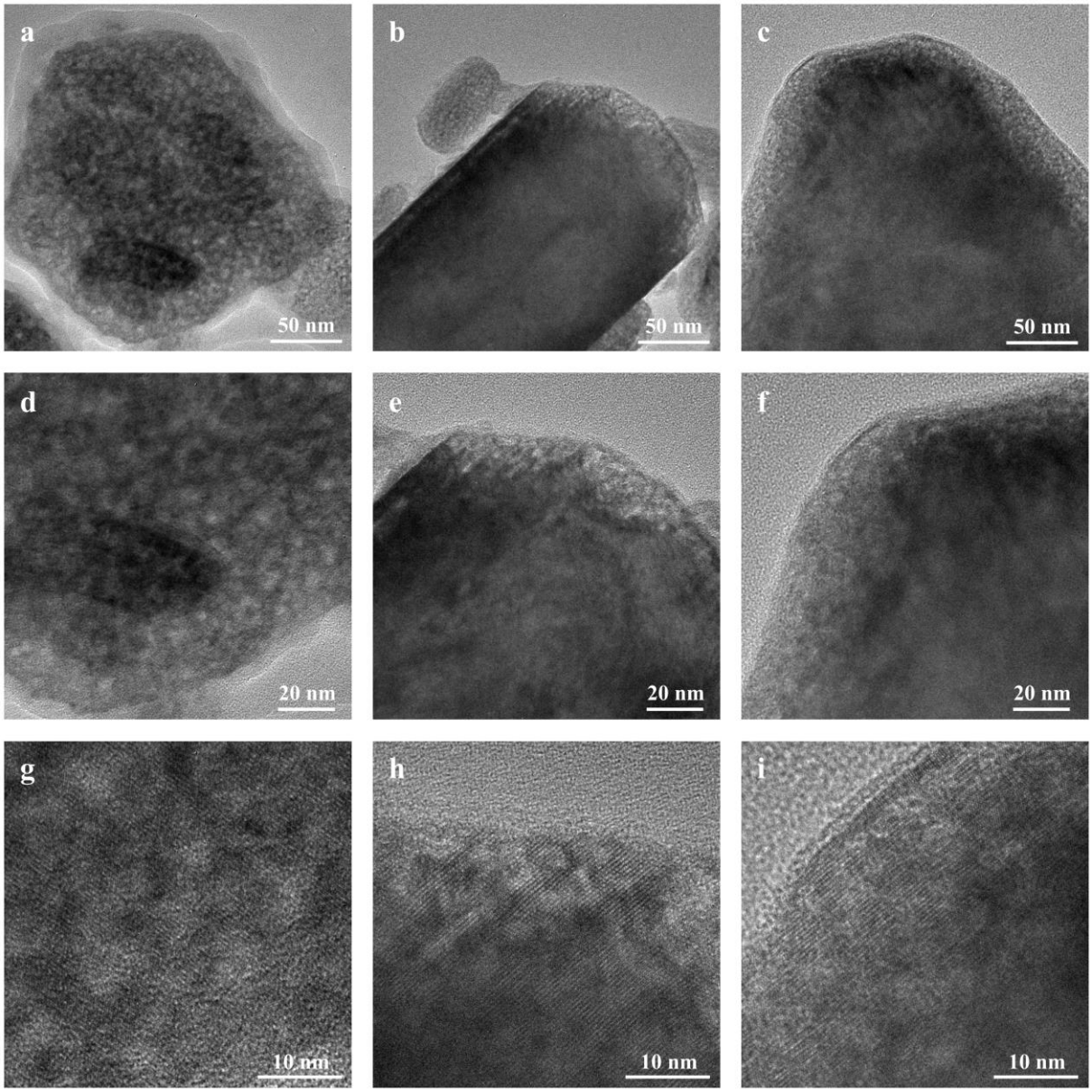

Fig. S14 TEM images of (a,d,g) B-LMO-600, (b,e,h) B-LMO-700 and (c,f,i) B-LMO-800 after 300 cycles at 1 C.

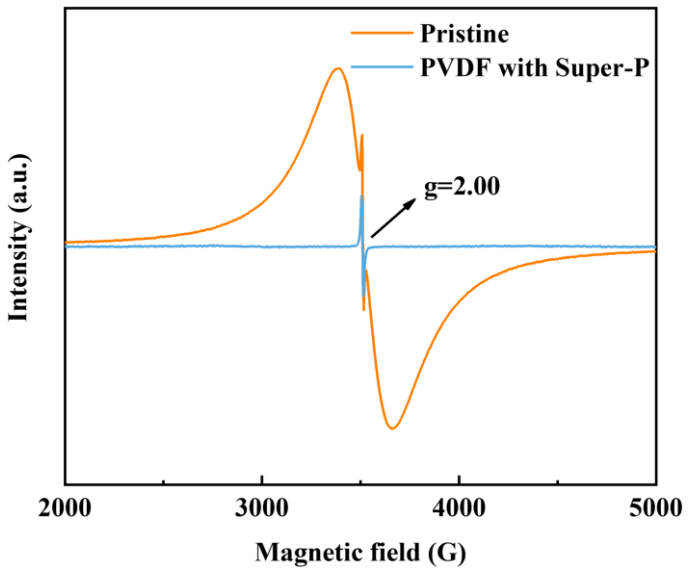

Fig. S15 EPR spectra for B-LMO-600 of Pristine and PVDF with Super-P electrodes. PVDF with Super-P represents that the electrode without active materials.

Table S1 Rietveld refinements results of XRD patterns for LMOs using a monoclinic *C2/m* space group.

Sample	a (Å)	b (Å)	c (Å)	β (°)	V (Å^3)	R_p
LMO	4.9243	8.5151	5.0204	109.1474	198.8701	9.49
B-LMO	4.9317	8.5305	5.0220	108.9420	199.8398	4.78
B-LMO-400	4.9296	8.5299	5.0203	109.0352	199.5602	5.69
B-LMO-500	4.9284	8.5340	5.0175	109.0488	199.4811	5.70
B-LMO-600	4.9262	8.5233	5.0178	108.9635	199.2562	7.26
B-LMO-700	4.9223	8.5245	5.0144	109.0436	198.8921	8.47
B-LMO-800	4.9269	8.5236	5.0218	109.1798	199.1891	9.89

Table S2 Cycling performances of B-LMO-400, B-LMO-500, B-LMO-600, B-LMO-700 and B-LMO-800 at 1 C, all cells were activated in three cycles at 0.1 C.

Sample	Discharge capacity ($mAh \cdot g^{-1}$)		Capacity retention (%)
	1 cycle	300 cycles	
B-LMO-400	52.3	22.5	43.0
B-LMO-500	54.1	30.3	56.0
B-LMO-600	103.3	42.1	40.7
B-LMO-700	71.9	36.2	50.3
B-LMO-800	35.0	40.9	116.8

References

1 J. Rana, J.K. Papp, Z. Lebens-Higgins, M. Zuba, L.A. Kaufman, A. Goel, R. Schmuch, M. Winter, M.S. Whittingham, W. Yang, B.D. McCloskey and L.F.J. Piper, *ACS Energy Lett*., 2020, **5**, 634-641.

2 Z. Zhuo, K. Dai, R. Qiao, R. Wang, J. Wu, Y. Liu, J. Peng, L. Chen, Y. Chuang, F. Pan, Z. Shen, G. Liu, H. Li, T.P. Devereaux and W. Yang, *Joule*, 2021, **5**, 975-997.